

Asteroseismology of the red giant companions to Gaia BH2 and BH3

DANIEL HEY ^{1,*} YAGUANG LI (李亚光) ^{1,†} AND J. M. JOEL ONG (王加冕) ^{1,‡}

¹*Institute for Astronomy, University of Hawaii, Honolulu, USA*

ABSTRACT

The stellar companions in the binary black hole systems Gaia BH2 and BH3, both of which are α -enhanced red giant branch stars, are expected to show normal modes with the characteristic signature of convectively-driven solar-like oscillations. We investigate this using photometry from the TESS mission and find such a signal for Gaia BH2. For Gaia BH2, we measure a power excess frequency of $\nu_{\max} = 60.15 \pm 0.57 \mu\text{Hz}$ and a large separation of $\Delta\nu = 5.99 \pm 0.03 \mu\text{Hz}$, yielding a mass of $1.19^{+0.08}_{-0.08} M_{\odot}$, which is in agreement with spectroscopically derived parameters. Seismic modeling favors an age for the red giant of $5.03^{+2.58}_{-3.05}$ Gyr, strongly suggesting that it is a young, α -enriched giant star, which are thought to arise from a binary accretion or merger scenario. Ground-based photometry of Gaia BH2 spanning 8 years indicates a photometric period of 398 ± 5 d, which we tentatively attribute to rotation. If this rotation is physical, it can not be explained solely by evolutionary spin-down or magnetic braking, and implies that the red giant underwent some tidal forcing mechanism. Suggestively, this period is close to the pseudo-synchronous spin period of $P_{\text{spin}} = 428 \pm 1$ days derived from the binary orbit. For Gaia BH3, we are unable to identify an asteroseismic signal in the TESS data despite predicting that the amplitude of the signal should lie well above the measured noise level. We discuss a number of scenarios for why this signal may not be visible.

1. INTRODUCTION

The recent astrometric discoveries of Gaia BH2 and BH3, the first binary systems consisting of a red giant star and a dormant black hole (El-Badry et al. 2023a; Gaia Collaboration et al. 2024), have challenged our understanding of binary black hole formation (Li et al. 2024; Gilkis & Mazeh 2024; Miller et al. 2024; Tanikawa et al. 2024; Kotko et al. 2024; Green et al. 2024; Marín Pina et al. 2024). In unveiling the formation mechanism of these systems, it is essential to accurately determine the fundamental properties (and in particular the mass and age) of the luminous component. This is because those of the compact component may often only be inferred from the luminous component, rather than being directly measurable. For example, if the orbits of these systems are characterized through astrometry, the reliability of the mass function (and therefore any estimate of the black-hole mass) crucially depends on the accuracy with which the stellar mass is measured.

Over the past century, variable stars have proven to be an invaluable resource in refining our understanding of stellar structure, evolution and fundamental stellar properties. Notably, the recent high-precision space photometry revolution, catalysed by the Kepler and TESS missions (Ricker et al.

2015; Chaplin et al. 2015; Guzik et al. 2016), has provided astronomers with an incredible amount of high-precision light curves spanning the entirety of the Hertzsprung-Russell diagram (HRD; Kurtz 2022). The richness of these data has paved the way for asteroseismology – the study of the internal structure of stars through their self-excited oscillations (Aerts et al. 2010; Aerts 2021).

No class of star has benefited more from our improved understanding of asteroseismology than red giants (Bedding et al. 2011), in which stochastically excited modes have been identified with amplitudes around 0.1 mmag and periodicities on the order of hours (e.g. Hekker 2018; Basu & Hekker 2020, for a review). These oscillations are driven by near-surface turbulent convection (e.g., Goldreich & Keeley 1977; Balmforth 1992), which both excites and damps modes around a characteristic power excess frequency (ν_{\max}) (Tassoul 1980). Excited pressure modes (p-modes) of equal angular degree and different radial order are spaced in frequency by the large separation ($\Delta\nu$) which is proportional to the mean density of the star (Ulrich 1986). Such normal modes have been measured in tens of thousands of red giants (Pinsonneault et al. 2014, 2018; Yu et al. 2018; Hon et al. 2021; Mackereth et al. 2021).

Asteroseismology has seen great success as a tool for characterizing other kinds of invisible stellar companions — most notably exoplanets (e.g. Deal et al. 2017; Lin et al. 2024; Huber 2018; Lundkvist et al. 2018; Huber et al. 2022; Nielsen et al. 2020). We extend this now to the recently discovered dormant black hole systems by Gaia. In two of these systems, Gaia BH2 and Gaia BH3, the luminous compan-

Corresponding author: Daniel Hey
dhey@hawaii.edu

* Not a Fellow

† Beatrice Watson Parrent Fellow

‡ Hubble Fellow

arXiv:2503.09690v1 [astro-ph.SR] 12 Mar 2025

ion has been conclusively shown to be a red-giant star (El-Badry et al. 2023a; Gaia Collaboration et al. 2024). The precise mechanism by which these systems form remains a mystery. However, as effectively all sufficiently evolved red giants oscillate, we investigate these stars for their asteroseismic potential. The asteroseismology of these luminous companions may prove a promising source of clues about the under-specified physical nature of their formation and history.

In this paper, we produce light curves from the TESS target pixel files of the stellar companions to Gaia BH2 and Gaia BH3 (hereafter, BH2* and BH3*). We find strong evidence of oscillations in BH2* at the frequency expected of stars with similar spectroscopic properties (Sec. 3.1), and a non-detection of oscillations in BH3* (Sec. 4.1). For BH2*, this enables a methodologically independent characterization of its fundamental properties, which we find to be in good agreement with existing published values. We also identify a photometric period in ground-based photometry which we tentatively suggest is caused by rotational modulation (Sec. 3.2). This period, the young asteroseismic age, and the fact that it is α -enhanced suggest that it has undergone interactions with a companion, which we discuss in Sec. 3.3. For BH3*, a non-detection suggests that the uncertainties on the stellar parameters reported in the discovery paper are potentially too narrow, or that the scaling relations are inaccurate for very metal-poor stars (Sec. 4.2). In particular, for the published mass we expect an asteroseismic amplitude above the noise level of the light curve. We discuss several scenarios as to why the signal could not be found, such as inaccurate scaling relations for metal-poor stars, and narrow uncertainties on the stellar properties.

2. DATA AND METHODS

2.1. Photometry

We used data from the Transiting Exoplanet Survey Satellite (TESS; Ricker et al. 2014). TESS photometry is taken with pointings fixed for 27 day at a time, corresponding to one sector. The observing strategy of the nominal and first two extended TESS missions is such that only photometry in single sectors, separated by two years at a time, is available for both BH2* and BH3*. For each sector of observation, we extract target pixel files using TESScut (Brasseur et al. 2019).

We extract the light curves from the TESS target pixel files in each sector using a regression corrector as implemented in `lightkurve` (Vinicius et al. 2018). Briefly, the regression corrector operates by removing scattered light by detrending the light curve against vectors which are predictive of the systematic noise. These vectors are created from Principal Component Analysis (PCA) of pixels outside the selected aperture, and assumed to be representative of the scattered light. The regression corrected light curve is then normalized by dividing its median, and a 3σ clipping is applied to remove significant outliers.

2.2. Global Asteroseismic Properties and Scaling Relations

The large sample sizes afforded by *Kepler* and *TESS* now allow the asteroseismic properties of stars, as a function of their stellar properties, to be understood to such an extent that we can predict the probability of detecting oscillations given a star’s mass, temperature, surface gravity, while taking into account instrumental considerations such as cadence of observations and detector coordinates (Schofield et al. 2019).

Kepler observations have demonstrated that the oscillation amplitudes of red giants satisfy a scaling relation that depends on mass, luminosity and temperature (Huber et al. 2011; Corsaro et al. 2013):

$$A_{\text{oscillation}} \sim \frac{L^s}{M^t T_{\text{eff}}^{r-1} c_K(T_{\text{eff}})} \quad (1)$$

where $s = 0.838$, $t = 1, 32$, $r = 2$, and

$$c_K \sim \left(\frac{T_{\text{eff}}}{5934\text{K}} \right)^{0.8}. \quad (2)$$

Moreover, the large frequency separation $\Delta\nu$ and frequency of maximum power excess ν_{max} of convectively-excited pulsations also scale with stellar properties like their masses, radii, and temperatures (Brown et al. 1991; Kjeldsen & Bedding 1995):

$$\begin{aligned} \frac{\nu_{\text{max}}}{\nu_{\text{max}\odot}} &\sim \left(\frac{M}{M_\odot} \right) \left(\frac{R}{R_\odot} \right)^{-2} \frac{T_{\text{eff}}^{-1/2}}{T_{\text{eff}\odot}} \quad \text{and} \\ \frac{\Delta\nu}{\Delta\nu_\odot} &\sim \left(\frac{M}{M_\odot} \right)^{1/2} \left(\frac{R}{R_\odot} \right)^{-3/2}, \end{aligned} \quad (3)$$

where the solar values are $\nu_{\text{max}\odot} = 3090 \pm 30 \mu\text{Hz}$, $T_{\text{eff}} = 5777 \text{K}$, and $\Delta\nu_\odot = 135.1 \pm 0.1 \mu\text{Hz}$.

Our observational characterization of these global seismic properties described below will rely primarily on existing automated software products, such as the PySYD pipeline Chontos et al. (2021) and PBJam (Nielsen et al. 2021).

3. GAIA BH2

BH2* (Gaia DR3 5870569352746779008, TIC 207885877) is a G=12.3 magnitude nearby ($d=1.16 \text{ kpc}$) star on the lower red giant branch, before the red clump. El-Badry et al. (2023a) infer a mass of $M_* = 1.07 \pm 0.12 M_\odot$, moderately subsolar metallicity ($[\text{Fe}/\text{H}] = -0.22 \pm 0.02$) and strong α enhancement ($[\alpha/\text{Fe}] = 0.26 \pm 0.05$), by fitting spectroscopic observations against evolutionary models. They suggest that the strong α -enhancement is primordial owing to the wide orbit of the system, but could also arise from pollution of low-velocity ejecta during a failed supernova.

BH2* was observed by TESS in sectors 11, 38, and 65 at cadences of 30 minutes, 10 minute, and 2 minutes respectively. Fig. 1. We use a 10×10 TESS pixel cutout, and show the target pixel file and light curve in Fig. 1. The region surrounding BH2* is moderately crowded, meaning that we must be careful when choosing an aperture. We experiment with multiple apertures centred on BH2*, permuting through every combination up to a 3×3 aperture. We find that the 3×3

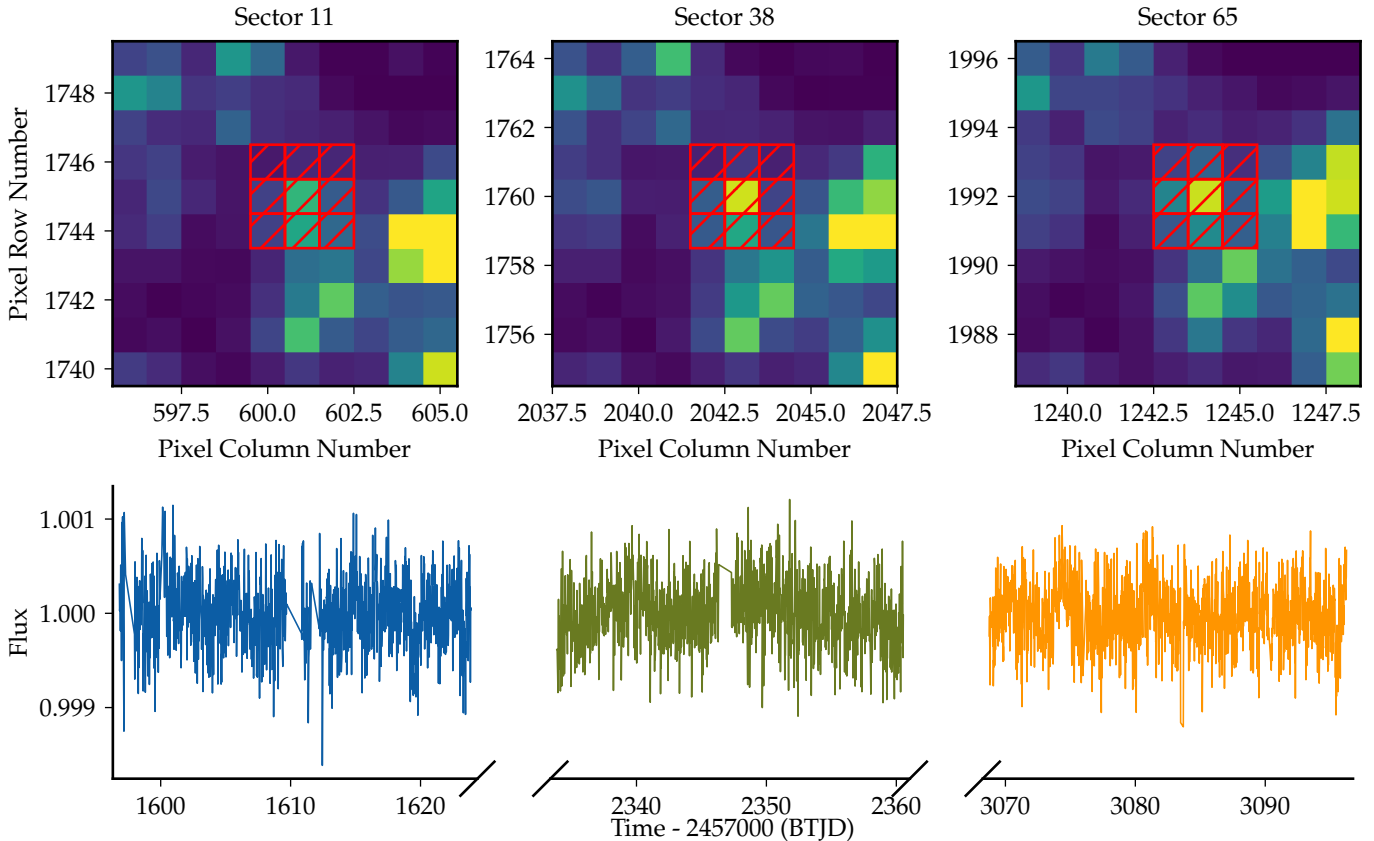


Figure 1. Top panel: TESS Target pixel file cutouts of the three sectors of Gaia BH2, with the selected aperture overlaid in red. Note the presence of potential nearby contaminants. Within two pixels of the selected aperture, there are no contaminants brighter than 13th Gaia magnitude beside BH2* itself. Bottom panel: Light curves from each sector obtained through regression correction. The light curves have been binned to a uniform 30-minute cadence, and outliers have been removed.

aperture best captures the asteroseismic signal with the highest SNR. Importantly, the signal shows up in every aperture which is centered around BH2*, and is unlikely to belong to a nearby target. The closest target of significance to BH2* is Gaia DR3 5870569318392555776, an A/F-type star which would be expected to have significantly higher amplitude and frequency of variability.

3.1. Asteroseismology

The power spectrum of BH2* is shown in Fig. 2, where we find a power excess corresponding to solar-like oscillations at frequencies between 50 to 80 μHz . The photometric data has a white noise level of 22 ppm at high frequencies. We use the PySYD pipeline to measure a ν_{max} of $60.15 \pm 0.57 \mu\text{Hz}$ and a large frequency separation $\Delta\nu$ of $5.99 \pm 0.03 \mu\text{Hz}$.

We also attempted to use PBJam for this purpose, which should in principle both be capable of deriving more precise estimates of $\Delta\nu$ and ν_{max} by fitting a template power spectrum of even-degree p-modes, as well as of estimating the frequencies of individual normal modes. This procedure yielded $\Delta\nu = 6.01 \pm 0.02 \mu\text{Hz}$ and $\nu_{\text{max}} = 61 \pm 1 \mu\text{Hz}$. However, the adverse S/N conditions of single-sector TESS data prevented PBJam’s automated procedures from deriving a robust mode identification, since it relies on the visibility of quadrupole

modes to distinguish between the most prominent $\ell = 0$ and $\ell = 1$ modes. Moreover, since this template-fitting procedure is constrained only by even-degree modes, it has less statistical support than would be obtained from also including the dipole modes. As such, we adopt the values reported by PySYD for our subsequent analysis.

Rather than resorting to mode identification by eye for such a low S/N power spectrum, we turn to lessons about the behavior of pulsating red giants that the asteroseismology community has learned from the Kepler sample. There are over 16,000 red giant stars observed by Kepler with measured asteroseismic properties (e.g. Yu et al. 2018). The majority of these stars have also been observed by TESS in multiple sectors and cadences. Using this, we can identify “twins” in the Kepler sample for any given red giant: Kepler targets with a similar apparent magnitude and ν_{max} as predicted from the published stellar parameters. We compared BH2* against all Kepler red giants in the consolidated APOKASC3 catalogue (Pinsonneault et al. 2024), quantifying similarity using the χ^2 statistic, incorporating constraints from metallicity, effective temperature, and $\Delta\nu$. This analysis identifies KIC 2712761 as the star with the lowest χ^2 discrepancy from BH2*. We will refer to it as BH2*’s “Kepler twin”.

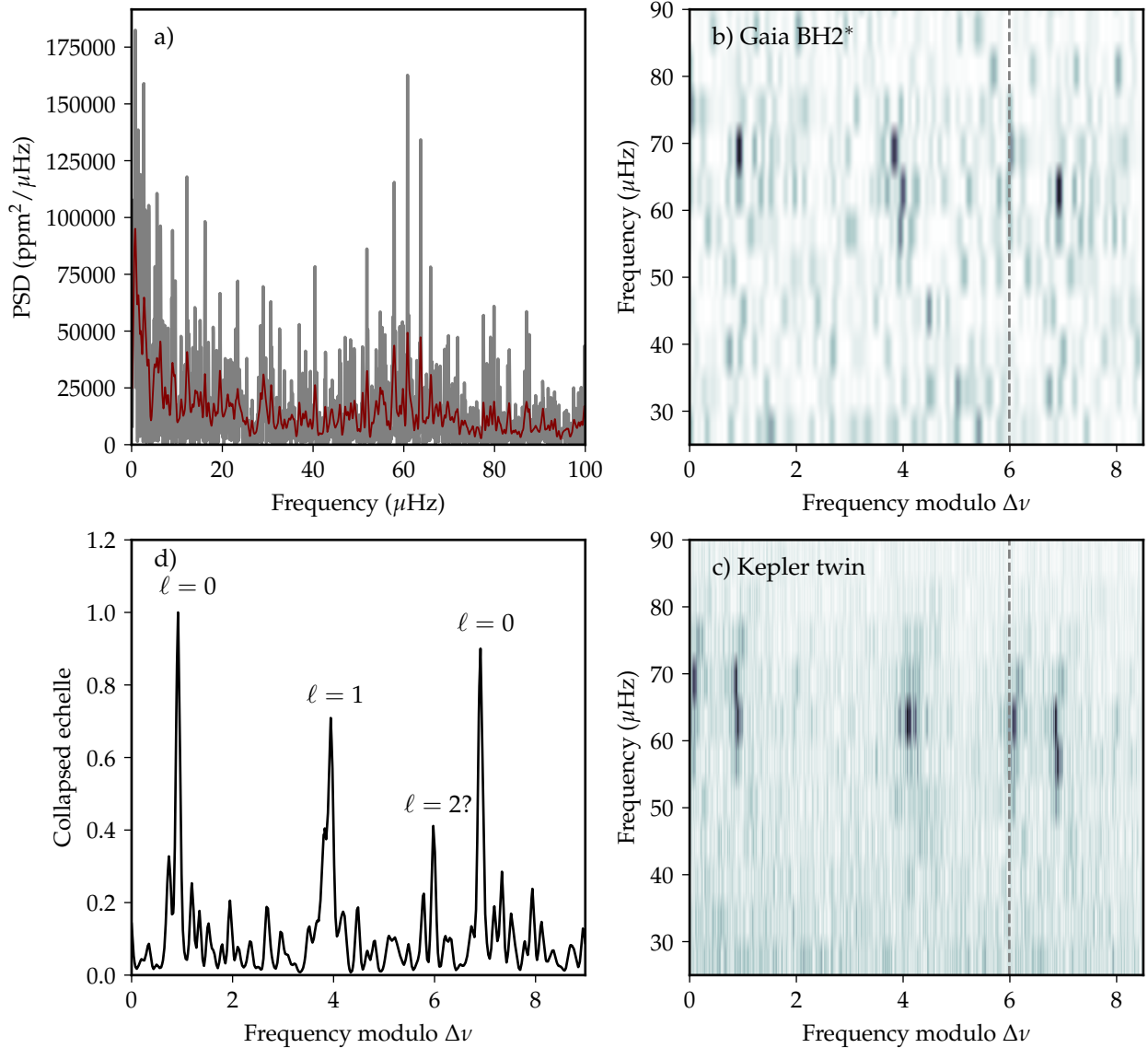


Figure 2. **a)** Power spectral density of BH2*, with the power excess around $60\mu\text{Hz}$. The red line is the power spectrum convolved with a Gaussian kernel of width $0.2\mu\text{Hz}$, highlighting the individual modes. **b)** The echelle diagram of the PSD at the measured $\Delta\nu$ (dashed line). **c)** The echelle diagram for a Kepler twin (see text), with similar stellar properties. **d)** The collapsed echelle diagram of BH2*, highlighting the radial, dipole, and quadrupole modes.

The frequency echelle diagram of the power spectrum of BH2* in comparison to its Kepler twin (Fig. 2) shows the oscillation modes forming three distinct ridges we consider to be the $\ell = 0$, $\ell = 1$, and $\ell = 2$ modes. This is corroborated by relying on relations between $\Delta\nu$ and the p-mode phase offset ϵ (White et al. 2011; Ong & Basu 2019). We measure the separation between the $\ell = 0$ and $\ell = 2$ ridges (the small separation; $\delta\nu_{0,2}$) using the collapsed echelle with a Monte-Carlo routine, finding a value of $0.93 \pm 0.05\mu\text{Hz}$.

El-Badry et al. (2023a) similarly extracted TESS light curves for BH2* in search of asteroseismic signatures, finding a weak detection of a signal with a peak frequency at $61\mu\text{Hz}$. While we confirm these results here, we are also able to further identify the large and small separations. The differ-

ence between their result and our unambiguous detection of oscillations is most likely due both to selection of the aperture and light curve extraction, as well as our having additional data at our disposal: at the time of their analysis, El-Badry et al. (2023a) did not have access to Sector 65 observations taken at 10 minute (rather than 30 minute) cadence, which greatly improves the S/N of the power excess.

To obtain stellar properties from our measured ν_{max} and $\Delta\nu$, we use the normalizing flow prescription outlined in Hon et al. (2024) using the software MODELFLows, based on asfgrid stellar models with corrected large frequency separations for lower metallicity (Sharma et al. 2016; Stello & Sharma 2022). In this method, stellar models are emulated using normalizing flows, allowing us to sample the poste-

<i>Gaia</i> BH2		
Measured quantities		
Power excess	ν_{\max} (μHz)	60.15 ± 0.57
Large separation	$\Delta\nu$ (μHz)	5.99 ± 0.03
Small separation	$\delta\nu_{0,2}$ (μHz)	0.93 ± 0.05
Photometric period	P_{phot} (day)	398 ± 5
Literature quantities[†]		
Temperature	T_{eff} (K)	4604 ± 87
Bolometric luminosity	L_* (L_{\odot})	24.6 ± 1.6
Surface gravity	$\log g$ (cm s^{-2})	2.71 ± 0.24
Radius	R_* (R_{\odot})	7.77 ± 0.25
Mass	M_* (M_{\odot})	1.07 ± 0.19
Metallicity	[Fe/H]	-0.22 ± 0.02
α -enhancement	[α /Fe]	0.26 ± 0.05
Derived quantities (asfgrid)		
Radius	R_* (R_{\odot})	$8.55^{+0.20}_{-0.15}$
Mass	M_* (M_{\odot})	$1.23^{+0.09}_{-0.09}$
Age	τ (Gyr)	$5.11^{+1.22}_{-1.78}$
Derived quantities (cnfgiant)		
Mass	M_* (M_{\odot})	$1.19^{+0.08}_{-0.08}$
Age	τ (Gyr)	$5.03^{+2.58}_{-3.05}$

Table 1. Measured, derived, and literature values of the red giant in the binary system Gaia BH2. Note that the radius is fixed for the cnfgiant grid because the luminosity and temperature are inputs. [†]From El-Badry et al. (2023a).

rior mass and radius of the star with our input measurements. Given that BH2* is α -enhanced ([α /Fe]= 0.26 ± 0.05), we correct the input metallicity using the prescription of Salaris et al. (1993) and obtain a corrected metallicity of $= -0.037 \pm 0.04$ dex.

Using our values from Table 1 and the measured temperature, we sample the stellar grid (asfgrid) for 5000 points with ‘evstate’ set to zero, corresponding to the red giant branch. We also make use of the cnfgiant grid available in MODELFLows, which is a narrower grid defined only for hydrogen shell-burning stars with $0.7 \leq M \leq 2.5M_{\odot}$. This grid allows us to incorporate the small separation and luminosity as constraints, which effectively fixes the radius of the star. We note that the small separation is significantly weaker as a diagnostic of internal structure for stars on the red giant branch compared to the main sequence (Ong et al. 2025), and so has little effect on our results – running the same grid without the small separation results in effectively identical results.

For the cnfgiant we find a mass of $1.23^{+0.09}_{-0.09} M_{\odot}$ and radius of $8.55^{+0.20}_{-0.15} R_{\odot}$. For the asfgrid we find a mass of $1.19^{+0.08}_{-0.08} M_{\odot}$. Both these masses are within 1σ of the liter-

ature value (El-Badry et al. 2023a), but the radius is slightly larger. Table 1 summarizes these results.

The larger uncertainty in age for the cnfgiant grid is a due to the larger number of free parameters, such as initial helium abundance, mixing length parameter, and convective core and envelope overshooting, which are unconstrained in this instance. The difference in ages between model grids is only 0.08 Gyr, and so we consider the systematic uncertainty to be very small. We adopt the age from the cnfgiant grid, which is produced solely for red giants; $\tau = 5.03^{+2.58}_{-3.05}$ Gyr. The model age confirms that BH2* is a young, α -enhanced star, if we assume no departures from canonical single-star evolution. We discuss these implications in Sec. 3.3.

3.2. Long-term photometric modulation

While relatively uncommon, many red giant stars are known to show long-term photometric modulation associated with rotation (e.g., Ceillier et al. 2017; Gaulme et al. 2014, 2020; Ong et al. 2024). Given that TESS’s short-sector observing strategy and instrumental systematics render it difficult to constrain signals with periods longer than the length of contiguous sectors (Colman et al. 2024; Clayton et al. 2024; Binks & Günther 2024), we instead determine these using the ASAS-SN (the All-Sky Automated Survey for Supernovae; Kochanek et al. 2017) light curves of BH2*. ASAS-SN is a ground-based network of observatories dedicated to transient science and long-term photometric variability. BH2* is in the ideal magnitude range for observations with ASAS-SN (Hart et al. 2023).

To separate true signals from potential systematics associated with ASAS-SN’s observing strategy and instrumentation, we also produce a light curve using the Asteroid Terrestrial-impact Last Alert System (ATLAS; Tonry et al. 2018). ATLAS is a ground-based mission with effectively daily cadence across the entire sky, with a pixel scale of 1.86". Although primarily a mission focusing on the northern hemisphere, ATLAS now also has cameras stationed in the southern hemisphere which can image stars at lower declination. We produce both difference and reduced photometry of BH2* using the ATLAS forced photometry server¹, which provides public access across the entirety of the ATLAS mission. Data processing and photometry are described in more detail in Tonry et al. (2018) and Smith et al. (2020). We also obtain approximately 8 years of ASAS photometry (ASAS-3; Pojmanski 1997) in the V-band. Manual inspection of the ASAS-3 data suggests a period of 426 days, however, the false alarm level of the signal is over 10% and so we do not include it in our analysis.

The ASAS-SN light curve of BH2* has an average uncertainty on each point of 0.005 mag. The light curve shows three clear periodicities at approximately 1500 d, 390 d, and 494 days above a 1% false alarm level (listed in order of decreasing amplitude) (Fig. 3). Given that the survey is ground-based, it is important to ensure that this signal is not a system-

¹ <https://fallingstar-data.com/forcedphot/>

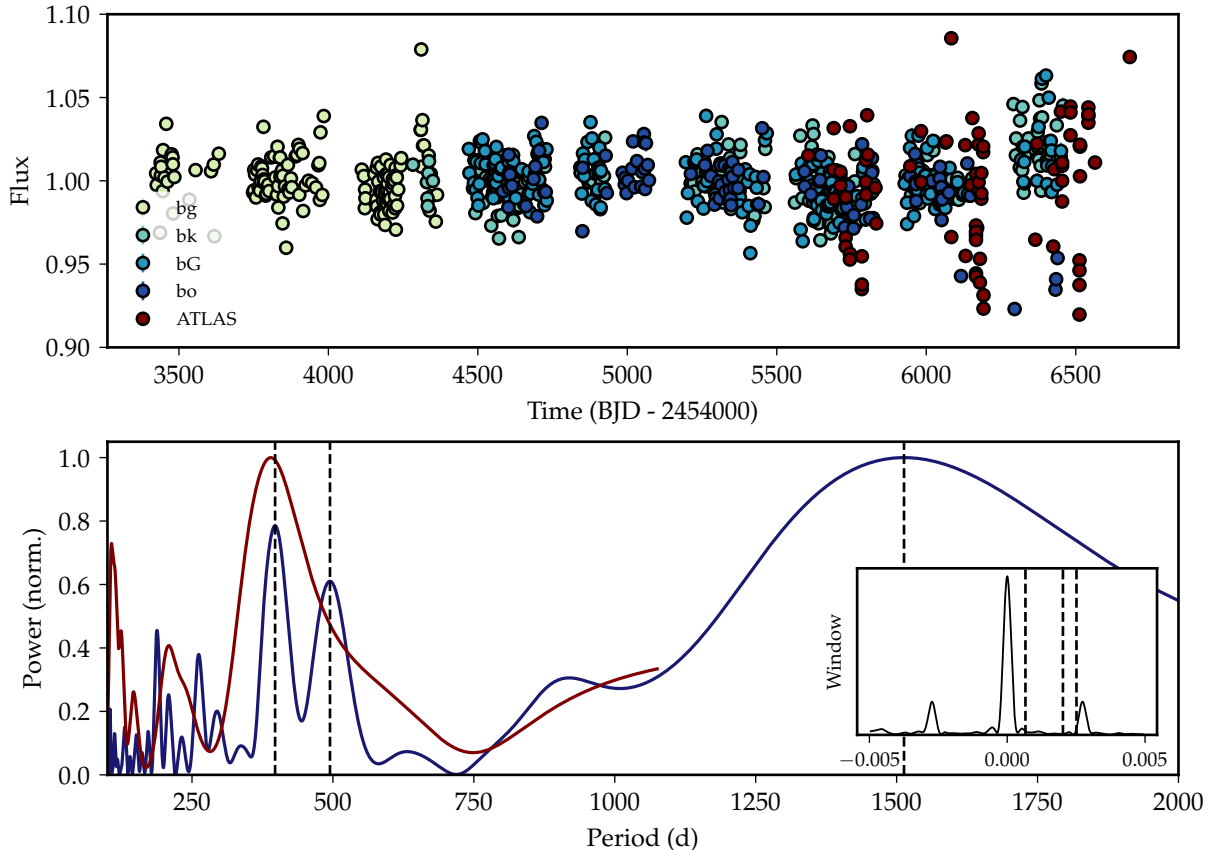


Figure 3. Top panel: ASAS-SN (blue) and ATLAS (red) light curves of BH2*. Each color for ASAS-SN represents a different camera in the network, each of which have their own offset which has been median divided out. Bottom panel: The power spectrum of the ASAS-SN and ATLAS light curves respectively. The dashed black lines indicate measured periods at 397 d, 495 d, and 1513 d. The inset on the bottom panel shows the window function (in frequency, d^{-1}), with a signal at Earth’s orbital frequency ($1/365$) d^{-1} . There are no peaks in the ASAS-SN window function associated with our measured periods (black dashed lines).

atic artifact of the survey, such as being an alias of the Earth’s diurnal, annual, or lunation frequencies. We therefore inspect the observational window function for the ASAS-SN power spectrum, shown inset in the bottom panel of Figure 3. We find that these three periodicities do not correspond to any sidelobes of this window function, suggesting that they are astrophysical rather than systematic in origin. We also perform the same analysis after applying Gold deconvolution to suppress sidelobes in the spectral window function of the data (Morháč 2006; Li et al. 2025). The deconvolved spectrum shows the same periodicities. We measure these periods by fitting a sine wave with a flux offset to the light curve using EMCEE for 5000 tuning steps and 5000 draw steps. We fit only the ASAS-SN light curve, because the ATLAS data has significantly larger scatter. We find periods of 398 ± 5 , 494 ± 9 , and 1513 ± 65 days.

Given the crowded field, it is again possible that the signal is contaminated from nearby stars even though ASAS-SN has a smaller pixel scale (8") than TESS (21"), and ATLAS is even smaller (1.86"). There are 19 stars within 20" of BH2* according to Gaia DR3, with the brightest companion at 16th Gaia magnitude, in comparison to BH2* itself which is at

12.3th Gaia magnitude. The remaining majority of companions are around 20th Gaia magnitude, which would be too faint to measure photometric variations with ASAS-SN. We construct light curves of nearby stars and find no matching signal at the photometric periods we measure.

In summary, both the ASAS-SN and ATLAS data products indicate the presence of quasi-periodic photometric variability with a common period of $P_{\text{phot}} = 398 \pm 5$ d. This is far slower than both the fundamental period of BH2*’s oscillations (~ 0.2 d), as well as the correlation timescale of convective granulation in its envelope. Rather than stellar-astrophysical processes, we instead investigate if this might be attributable to any of the characteristic timescales associated with BH2*’s tidal interactions with its black hole companion. For example, the presence of a binary companion in a close orbit might endow it with faster rotation than we might ordinarily expect from a comparable isolated red giant (Zahn 1977).

Notably, BH2* is in an eccentric orbit with $e = 0.5176 \pm 0.0009$. Under such circumstances, Hut (1981) describes how tidal torques might spin BH2* up to rotate more quickly than the orbital period: these torques would be much stronger

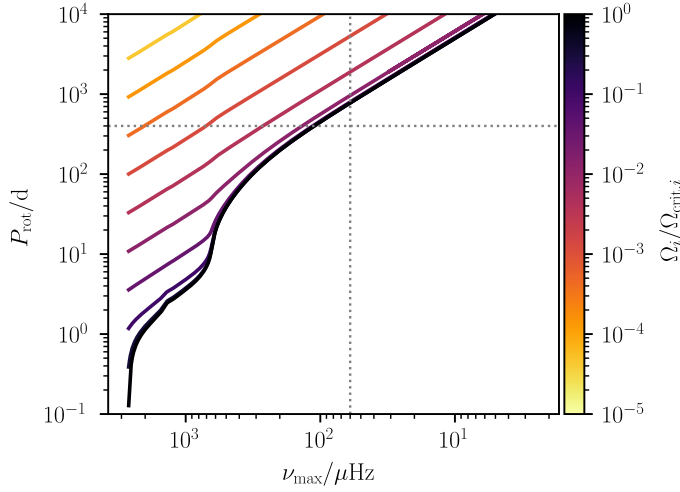


Figure 4. The photometric rotational period of BH2* is unlikely to have arisen without tidal forcing. Here we show the rotational evolution of MESA stellar models initialized at various fractions of the ZAMS breakup rotational frequency, indicated by the colourmap. Magnetic braking (calculated here using the prescription of van Saders & Pinsonneault 2013) causes stellar rotation to slow over evolutionary timescales, shown here using ν_{\max} as an age proxy. No other sources of angular momentum loss (such as mass loss) are accounted for in this simulation. Even under this extremely permissive scenario, our putative photometric rotation period (horizontal line) at the present day (vertical line) is faster than permitted by if BH2*'s rotation were to be attributed entirely to its primordial angular momentum.

near periastron (where the orbital frequency is fastest) than at apoastron. Thus, the average torque over the course of the orbit arises primarily from contributions close to periastron. As such, in addition to the mean orbital period ($P_{\text{orb}} = 1276.7 \pm 0.6$ d), this yields two other characteristic periods:

- The orbit-averaged torque vanishes when BH2* rotates at the “pseudosynchronous” period

$$P_{\text{pseud}} = \frac{(1 + 3e^2 + \frac{3}{8}e^4)(1 - e^2)^{\frac{3}{2}}}{1 + \frac{15}{2}e^2 + \frac{45}{8}e^4 + \frac{5}{16}e^6} \cdot P_{\text{orb}}, \quad (4)$$

rather than at the orbital period. Evaluating this expression with the reported values of the orbital period and eccentricity yield $P_{\text{pseud}} = 428 \pm 1$ d.

- Without assuming that BH2*'s rotation has been captured into pseudosynchronous resonance, we also note that its rotation period is strictly bounded from below by the rotational period associated with the angular frequency at periastron,

$$P_{\text{min}} = \frac{(1 - e^2)^{\frac{3}{2}}}{(1 + e)^2} P_{\text{orb}} = 347 \pm 1 \text{ d}. \quad (5)$$

We find that P_{phot} is of intermediate value between the minimum and pseudosynchronous period, and much closer to the latter than the former: this is highly suggestive of an interpretation of it being BH2*'s rotation rate. Such a fast rotation rate would be compatible with BH2* being either a single star or a merger remnant. In the single-star scenario, this rotation must necessarily result from tidal forcing, since it is too fast to have originated from its primordial angular momentum (Figure 4). Conversely, if BH2* were to have been a merger remnant, this would result from magnetic braking stalling when the rotation rate comes into pseudosynchronisation.

In either case, if indeed this quasi-periodic variability should be attributable to stellar rotation, this would also explain the relatively low visible amplitudes of the non-radial modes that we observe in BH2*, compared to the radial modes. Photometric variability would only trace rotation through the emergence of features on the stellar surface, such as spots originating from magnetic activity, which produce photometric modulations as they are rotated onto and off the visible disc. Such magnetic fields would have the effect of stabilizing convective flows, as does the rotational motion itself; both effects are known to suppress the oscillation amplitudes (Bonanno et al. 2014, 2019; Gaulme et al. 2020; Corsaro et al. 2024), and more strongly at higher angular degree.

The 10-year ASAS-SN data set also exhibits a second peak in its power spectrum, at $P_{\text{long}} \sim 1500$ d, which may also be a candidate rotation period. However, it is less easy to explain how such a rotational period could have arisen, since it is longer than the present orbital period, and does not correspond to either of the equilibrium timescales described above. To see why, we note that in addition to these, we in principle also have a hierarchy of secular-evolution timescales, associated with rotational (pseudo)synchronisation, tidal inspiral, and tidal circularization, ordered as $t_{\text{sync}} \sim (a/R)^6 < t_{\text{decay}} \sim (a/R)^{13/2} < t_{\text{circ}} \sim (a/R)^8$ (Zahn 1977; Hurley et al. 2002; Lai 2012).

Achieving a rotation period of P_{long} could be possible under the single-star scenario if we were to demand that t_{sync} were marginally faster than the rotational braking timescale of roughly 10^7 yr, in order to spin it up tidally beyond the otherwise negligible rotation rates that it would ordinarily possess this far up the red giant branch, while also avoiding capturing it into pseudosynchronisation. However, since $t_{\text{decay}} \sim 10t_{\text{sync}}$, this would also imply in-spiral on timescales comparable to that of evolution up the red giant branch, of roughly 10^8 yr. Coupling BH2* to tidal spin-up as a canonical single star, while avoiding runaway inspiral, would therefore only be possible with considerable fine-tuning of these timescales. If instead BH2* were to be a merger remnant, we would instead require t_{sync} to be much longer than the braking timescale, so that the initially rapid rotation after the merger does not stall in its braking when near pseudosynchronisation. However, since mass transfer rapidly circularizes orbits, this would require there to historically have been essentially no mass transfer from the black hole progenitor to BH2*, or its own progenitors.

Either way, while one would identify the additional appearance of P_{phot} as being the 4th harmonic of the rotational period if P_{long} were to signify rotation, it would be difficult to explain why other lower harmonics are not present in the power spectrum. Conversely, if we were to identify P_{phot} as the rotation period, a longer-period signal might be attributable to the timescales over which the spot morphologies change, or to latitudinal differential rotation.

As such, we believe it would be more plausible to interpret P_{phot} , rather than P_{long} , as being representative of BH2*'s present rotation rate. If this period is indeed the rotational period of the star then it corresponds to an equatorial velocity of $v_{\text{eq}} = 0.99 \text{ km s}^{-1}$ and equivalent $v \sin i$ assuming the star is seen equator-on. The influence in the line-broadening of the spectrum of the star would be minimal to non-existent, especially considering that El-Badry et al. (2023a) model an upper limit on $v \sin i$ of $< 1.5 \text{ km s}^{-1}$. Otherwise, we defer a more detailed investigation of possible secular evolution to future work when more photometric data is available.

3.3. Is Gaia BH2* a merger product?

Our asteroseismic model age requires that the red giant in Gaia BH2 belongs to the class of young ($< 8 \text{ Gyr}$), α -enriched red giants in the solar neighborhood. Such stars show an unusually high abundance of α elements, characteristic of thick disk stars, but are otherwise known to be young (Martig et al. 2015; Chiappini et al. 2015; Silva Aguirre et al. 2018; Clayton et al. 2020; Das et al. 2020; Zinn et al. 2022; Pinsonneault et al. 2024; Zhang et al. 2021). One possible interpretation of these stars is that they may be products of mass transfer or merger events. That is, they have a higher mass than they began with, and so appear younger when their ages are estimated assuming canonical single-star evolution (Zhang et al. 2021; Yu et al. 2024; Lu et al. 2024; Grisoni et al. 2024). Miglio et al. (2021) suggest that the occurrence rate of massive ($> 1.1 M_{\text{sun}}$) alpha rich red giants is on the order of 5% for the RGB, and significantly higher in the RC.

El-Badry et al. (2023a) consider the possibility of BH2* having been chemically enriched through pollution from the BH progenitor, since such enhancement is also seen in the donor stars of BH X-ray binaries. They argue, from geometric considerations, that the observed α -enhancement is unlikely to have arisen by the accretion of supernova ejecta. Instead, they suggest it is possible that low velocity ejecta remained gravitationally bound to the star and eventually accreted.

It is also possible that BH2* was enriched by interactions with the progenitor star itself, before core-collapse. For an assumed progenitor mass of $> 25 M_{\odot}$ (Sukhbold et al. 2016; Raithel et al. 2018), such a star would exceed the current orbital separation of the binary (4.96 AU). This common envelope evolution is disfavored, as it significantly reduces the orbital separation to much lower than what it is today (El-Badry et al. 2023b).

Merger remnants, or planetary engulfment, are also one explanation for the existence of rapidly-rotating red giants with no obvious stellar companions (e.g. Phillips et al. 2024;

Ong et al. 2024; Rui & Fuller 2024). Tidal synchronization (which we discuss above) may serve to brake initially rapid rotation more quickly than would magnetism alone, while at the same time also producing extra tidal heating that may continue to puff the star up even after after many Kelvin-Helmholtz timescales have elapsed.

This being so, it is tempting — considering the asteroseismic age of $5.03^{+2.58}_{-3.05} \text{ Gyr}$, its α -abundance, and apparently rapid rotation — to suggest that BH2* has undergone significant interactions with a past companion: either the progenitor to the present black hole, or another star. There are few chemical tracers we can use to support this theory, however. Lithium is widely quoted as a marker of recent engulfment or interaction events, because it is easily disrupted near the stellar envelope (Sayeed et al. 2024). However, Li is also depleted in a red-giant after the first dredge-up. There are still some red giants that show anomalously high Li abundance, but BH2* is not one of them (Tayar et al. 2023).

In addition to these chemical, rotational, or kinematic tracers of mergers or accretion, asteroseismic signatures of them also exist (e.g. Li et al. 2022b; Henneco et al. 2024): further asteroseismic measurements, with longer data sets, may prove helpful in determining whether BH2* has undergone such a previous history. For example, while we have been able to detect standing acoustic waves (p-modes) with the TESS data that we have in hand, all nonradial p-modes are known to couple to standing buoyancy waves (g-modes) that are otherwise trapped in the radiative cores of red giants (e.g. Shibahashi 1979; Unno et al. 1989; Beck et al. 2011), to produce gravitoacoustic mixed modes.

We have so far only been capable of measuring the most p-dominated of these mixed modes in BH2*. *Kepler* data show that, in addition to these p-mode features, a sufficiently long observing baseline might enable the measurement of the dipole g-mode period spacing $\Delta\Pi_1$ in comparably evolved stars (e.g. Vradar et al. 2016), among other features. Remarkably, single stars are bounded by a tight sequence in the $\Delta\nu$ - $\Delta\Pi_1$ diagram that is set by core electron degeneracy (Deheuvels et al. 2022) — we might therefore expect BH2* to lie on this sequence, given that its mass suggests it possesses an electron-degenerate core. If a red giant should lie in the forbidden region on this diagram — i.e. be more puffed up than expected of an ordinary red giant with a given electron-degenerate core size — then this is thought to be one indicator that its exterior may have been modified by physical processes not ordinarily accounted for in canonical stellar evolution, as would indeed be the case in the event of a merger (Rui & Fuller 2021) or mass accretion. As such, a period-spacing measurement would afford us a model-independent diagnostic of such noncanonical evolution, and serve as a test of whether we ought to consider this model age to be reliable. More photometric data could thus conclusively determine the evolutionary history of BH2*.

4. GAIA BH3

BH3* (Gaia DR3 4318465066420528000, TIC 73788466) is a high proper motion star, with its absolute magnitude and

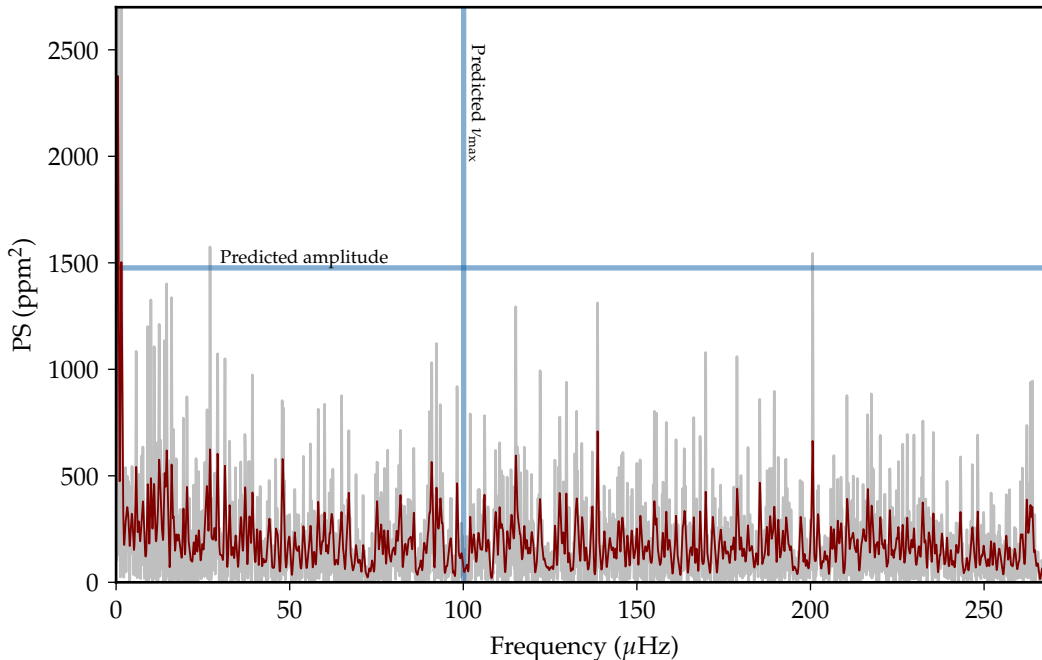


Figure 5. Power spectrum of BH3*. The red line is the power spectrum convolved with a Gaussian kernel of width $0.2\mu\text{Hz}$, to highlight the absence of any significant signal. The blue vertical and horizontal lines correspond to the predicted power excess and power of the asteroseismic signal.

color identifying it as ascending the red giant branch. In *Gaia* Collaboration et al. (2024), it was discovered to be host to a dormant $33M_{\odot}$ black hole in a wide ($P = 4195 \pm 112$ d) eccentric ($e=0.73$) orbit, with the black hole having extremely low near-infrared emission (Kervella et al. 2025). BH3* has been observed by TESS in two non-contiguous sectors, 54 and 81 at a cadence of 10 and 2 minutes respectively.

The stellar abundance analysis of BH3* identified it as extremely metal-poor ($[\text{Fe}/\text{H}] = -2.56 \pm 0.11$) and moderately α -enhanced ($[\alpha/\text{Fe}] = 0.43 \pm 0.12$). Interestingly, the authors note a lack of ^{13}C and solar levels of $[\text{Ba}/\text{Fe}]$, indicating that the star has not been chemically enriched by a companion star in the AGB phase. Given that it has evolved in apparent isolation, the asteroseismic properties of the star should be normal, conforming to what we understand of how these properties vary over time.

The star itself was carefully modeled by *Gaia* Collaboration et al. (2024). Notably, the reported stellar mass ($0.76 \pm 0.05M_{\odot}$) is extremely precise given that it was derived through isochrones. Since the stellar evolution models of stars clump up on the red-giant branch, and as noted by Tayar et al. (2022), isochrone uncertainties in mass for red-giant stars are typically much larger. We show, later on, that this mass uncertainty is almost entirely due to the tight age and luminosity priors placed on the star.

Given the moderately crowded region and high proper motion of *Gaia* BH3, we extract a 20×20 target pixel file for both sectors of observation. We follow the same regression correction method outlined in Sec. 2 with a 3×3 aperture, PCA comprising six components, and bin the light curve to a 30 minute cadence.

4.1. Asteroseismology

BH3* shows no obvious signs of asteroseismic variability, even after permuting both the aperture and number of PCA components (Fig. 5). There is a small increase in noise around $100\mu\text{Hz}$ which could possibly be interpreted as stochastic variability. We discuss now the absence of this signal, and possible causes.

As in Section 3, we search for Kepler light curve twins for BH3*. We compare it against the twin based on the implied ν_{max} and $\Delta\nu$ obtained from the asteroseismic scaling relations (Eq. 3). The goal of this exercise is to demonstrate that for the measured stellar parameters of BH3* in *Gaia* Collaboration et al. (2024), the TESS light curve of a known Kepler star at a similar magnitude should show a clear signal.

Using the stellar parameters in *Gaia* Collaboration et al. (2018), under the assumption that they are normally distributed, we predict $\nu_{\text{max}} = 100.3 \pm 1.0\mu\text{Hz}$. However, in metal-poor stars the ν_{max} scaling relation can be systematically off by up to 20% (e.g., Huber et al. 2024; Chaplin et al. 2020; Li et al. 2022a). In Yu et al. (2018), there are 83 Kepler stars within 1σ of this value at various magnitudes, and one Kepler star at a similar magnitude; *KIC* 8110811 (*TIC* 272270985, *Gaia* DR3 2079577161336956416). *KIC* 8110811 has been observed in sectors 14, 15, 41, 54, 55, 74, 75, 81, and 82 in cadences of 30 minutes, 10 minutes, and 2 minutes. Fortunately, two of these sectors (54 and 81) overlap with the TESS observations of BH3* and so should have similar, but not identical, noise properties. We calculate a TESS light curve of this target using identical methods as discussed in Sec. 2 across these overlapping sectors. We find

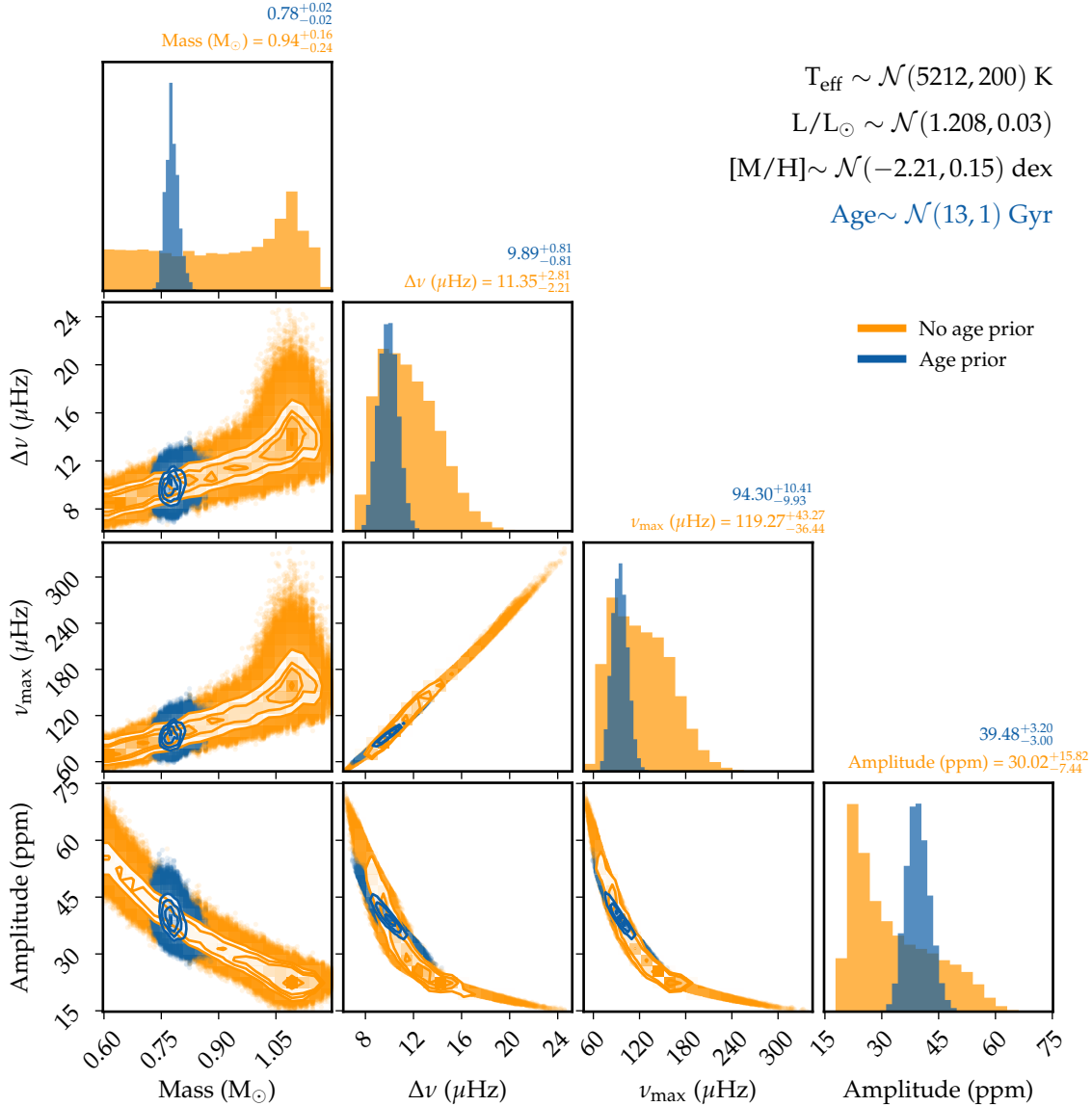


Figure 6. Posteriors of stellar properties of BH3* sampled from the stellar models, with temperature, luminosity and metallicity priors (orange), and with an additional age prior (blue).

that the signal is observable at the predicted amplitude given Eq. 1. The noise level of this twin light curve is slightly lower than that of BH3*, 9.3 ppm vs. 10.7 ppm, so it is more likely that the predicted amplitude is incorrect for metal-poor stars.

Of course, it is impossible to prove the absence of a signal despite our best efforts. There are other factors that could hinder detection of the expected $100 \mu\text{Hz}$ power excess. The most obvious of these is contamination. Gaia BH3 lies at such a low Galactic latitude (-3.5°) that there are several nearby stars, albeit at fainter magnitude. Given the $21''$ pixel scale of TESS, it is possible that the signal is diluted by companion stars, which we now investigate.

In the 20×20 target pixel file, there are 107 targets brighter than 16th magnitude, but only 6 targets brighter than 13th magnitude (including BH3*). Within the aperture we selected for producing the light curve there is only one other

target at 14th magnitude. This target, and the other fainter targets, if they are red giants, have effectively zero probability of showing oscillations in the TESS light curve due to their relative faintness.

The closest star of similar magnitude to BH3* is *Gaia* DR3 4318465032060792064, at a distance of $56.27''$ (approximately 3 TESS pixels). This star's color and luminosity imply that it belongs to a more evolved region of the red giant branch. Given the stellar properties from the *Gaia* DR3 catalog ($T_{\text{eff}} = 4905 \text{ K}$, $\log g = 2.5 \text{ dex}$), the star would be expected to be variable at a much lower frequency of $\sim 40 \mu\text{Hz}$ than what we expect in BH3*.

4.2. Stellar models

We computed a grid of stellar models using Modules for Experiments in Stellar Astrophysics (MESA, version r24.03.1;

Paxton et al. 2011, 2013, 2015, 2018, 2019; Jermyn et al. 2023). Adiabatic oscillation frequencies were calculated with GYRE (version 6.0.1; Townsend et al. 2013) using the structure profiles from MESA. The models incorporate elemental diffusion, an Eddington-gray atmospheric boundary condition (Eddington 1926), and exponential convective overshoot at convective envelope boundaries, and a moderate amount of mass loss $\eta = 0.2$ following Reimers’ prescription (Reimers 1975). The relative metal abundances follow the solar composition of Asplund et al. (2009), with additional α -element enrichment to match the observed value of $[\alpha/\text{Fe}] = 0.4$.

The initial helium abundance is set to $Y = 0.248$, consistent with the primordial value (Planck Collaboration et al. 2016). Large frequency separations ($\Delta\nu$) were computed using radial modes. We sampled the parameter space uniformly over mass $M \in (0.6, 1.2)M_{\odot}$, metallicity $[\text{Fe}/\text{H}] \in (-3.2, -2.4)$, and the mixing length parameter $\alpha_{\text{MLT}} \in (1.5, 2.5)$.

Gaia BH3 was recently discovered to belong to the metal-poor disrupted ED-2 stellar stream (Dodd et al. 2023; Balbinot et al. 2023, 2024), a substructure that forms a dynamically cold stellar stream which crosses the solar neighborhood. The near-zero spread in metallicity in ED-2 indicates that it was originated by a disrupted star cluster. This argument is in good agreement with the color-magnitude diagram (cf. fig 1 of Balbinot et al. 2023), which is well fitted with an extremely old single stellar population. The CMD of ED-2 closely resembles that of the GC M92 at an age of 13.80 ± 0.75 Gyr (Ying et al. 2023) with a slightly fainter main-sequence turn-off, indicating that BH3* is potentially older than 13 Gyr. This is consistent with the stellar modeling performed in the discovery paper (Gaia Collaboration et al. 2024), where the de-reddened Gaia colors of BH3* were fit to isochrones of 12 and 14 Gyr.

From the stellar models, it is obvious that the mass (along with other stellar parameters) is heavily constrained by the assumed age of the star (Fig. 6). Under only metallicity, luminosity, and temperature constraints, the mass of the star is not constrained (as expected). Given that the amplitude of the oscillation signal depends on the mass of the star, the higher mass implies a lower amplitude signal for the same ν_{max} . When using the age constraint of 13 ± 1 Gyr, the parameters are tightly constrained, similar to what was found in Gaia Collaboration et al. (2024). Most interestingly however, the predicted amplitude is constrained to a narrow region corresponding to 38 ± 3 ppm (Eq. 1). This is significantly higher than the median noise level of the power spectrum in the range corresponding to the expected power excess (12 ppm). We also used eq. 19 of Corsaro et al. (2013), who provide a separate scaling relation for the amplitudes. Using this, and the stellar models, we predict an even higher amplitude of 50 ± 6 ppm. Given that we do not detect a signal at either of these levels, it is possible that uncertainty on the luminosity is underestimated.

Finally, we consider one more scenario for why the predicted signal is not found. The predicted amplitude (Eq. 1) is scaled from the Kepler data, of which there are only a hand-

ful of extremely metal-poor stars. It has also been shown that metallicity can weakly affect the observed mode amplitudes (cf. figure 12 of Yu et al. 2018). It is possible, then, that the metal-poor nature of BH3* has caused us to substantially over-predict its oscillation amplitudes.

Regardless, even a detection of only ν_{max} and $\Delta\nu$ for BH3* may not be particularly useful for obtaining stellar parameters. As Huber et al. (2024) note, the asteroseismic scaling relations seem to break down in accuracy for very metal-poor ($[\text{Fe}/\text{H}] < -1$) stars. While constraints on stellar parameters by individual mode-frequency analysis and seismic modeling do remain extremely precise in these situations (e.g. Chaplin et al. 2020; Huber et al. 2024), this would only be achievable if an improved signal to noise ratio at either a shorter cadence, longer time baseline, or both, were to enable the measurement of individual mode frequencies. Given that we have not detected even a power excess (let alone individual modes), and that BH3* will not fall on any TESS silicon for the foreseeable future (Burke et al. 2020), there is little chance of performing such an analysis without dedicated follow-up.

5. CONCLUSION

We have investigated the TESS and ground-based light curves of the luminous companions in Gaia BH2 and BH3 for their expected signatures of seismic variability and potential rotational modulation. Our main conclusions are as follows.

- We identify an asteroseismic signal in Gaia BH2* with $\nu_{\text{max}} = 60.15 \pm 0.57 \mu\text{Hz}$ and a $\Delta\nu$ of $5.99 \pm 0.03 \mu\text{Hz}$. These global asteroseismic parameters yield a mass of $1.19^{+0.08}_{-0.08} M_{\odot}$, which is in excellent agreement with El-Badry et al. (2023a). With only a few TESS sectors of data, we are unable to perform detailed mode identification and modeling.
- The asteroseismic age measured for BH2* is $5.03^{+2.58}_{-3.05}$ Gyr, placing it as a member of the young, α -enhanced red giants. This population is suspected to be formed from merger or accretion events, enriching their α elements and increasing their mass.
- The long-term ASAS-SN light curve of BH2* shows three strong signals of periodicity at 397 d, 495 d, and 1513 days. The ATLAS light curve also shows evidence of photometric modulation at the 397 day period, although longer periods can not be determined given the shorter time coverage of ATLAS. If the signal at 397 d is due to rotational modulation, then it implies that BH2* was spun up through some tidal forcing mechanism. That is, the rotation period is faster than permitted by magnetic braking is BH2*'s rotation period were to be attributed entirely to its primordial angular momentum. We caution that this rotation period is tentative, and requires more follow-up to confirm.
- The pseudo-synchronous period inferred from the orbit of BH2* is $P_{\text{spin}} = 428 \pm 1$ days, which is close to

the measured period in the ground-based photometry. This indicates that BH2* was potentially spun up in its evolutionary history.

- BH2* will be observed by TESS in several more sectors over the next few years, after which point individual mode identification and detailed seismic analysis should be possible. This modeling will only serve to improve the age and should indicate whether BH2* is indeed a merger product.
- We detect no signature of asteroseismic oscillations in BH3*, despite strong constraints on the expected frequency and amplitude of variability. Given the noise level in the light curve, we predict that the expected amplitude should make this variability obvious.
- Given the absence of this signal, we compute a series of stellar evolutionary models based on the parameters from [Gaia Collaboration et al. \(2024\)](#). We suggest that either their extremely tight luminosity constraint should be relaxed to allow for a larger range of possible amplitudes and frequencies of oscillation, or that the amplitude scaling relations are too unconstrained at low metallicities. Our results do not change the inferred mass of the (BH3) black hole companion.

Our work demonstrates the utility of asteroseismology as a tool to characterize stellar properties, or to confirm the stellar properties obtained from other methods. The TESS mission has now observed a significant fraction of the entire sky, and the simplicity of producing light curves allows for asteroseismic analyses of brighter objects. Our key takeaway is that the red giant companion to Gaia BH2 is a young, α -enhanced star, with apparently rapid rotation. Both of these phenomena point to the red giant undergoing a merger or accretion

event in its past history, which could help constrain theories of dormant black hole binary formation mechanisms.

ACKNOWLEDGEMENTS

We thank Tim Bedding, Daniel Huber, Christina Hedges, and Joel Zinn for helpful comments and suggestions.

D. Hey acknowledges support from NSF (AST-2009828), NASA (80NSSC24K0621), and TESS GI Cycle 6 (80NSSC24K0506). Y. Li acknowledges support from Beatrice Watson Parrent Fellowship. J. M. J. Ong acknowledges support from NASA through the NASA Hubble Fellowship grant HST-HF2-51517.001, awarded by STScI. STScI is operated by the Association of Universities for Research in Astronomy, Incorporated, under NASA contract NAS5-26555.

This work has made use of data from the Asteroid Terrestrial-impact Last Alert System (ATLAS) project. The Asteroid Terrestrial-impact Last Alert System (ATLAS) project is primarily funded to search for near earth asteroids through NASA grants NN12AR55G, 80NSSC18K0284, and 80NSSC18K1575.

This paper includes data collected with the TESS mission, obtained from the MAST data archive at the Space Telescope Science Institute (STScI). Funding for the TESS mission is provided by the NASA Explorer Program. STScI is operated by the Association of Universities for Research in Astronomy, Inc., under NASA contract NAS 5-26555.

The playlist made while writing this paper is available [here](#).

Facilities: TESS, ASAS-SN, ATLAS

Software: [astropy \(Astropy Collaboration et al. 2013\)](#), Modules for Experiments in Stellar Astrophysics MESA ([Paxton et al. 2011, 2013, 2015, 2018, 2019](#); [Jermyn et al. 2023](#)), TESS-point ([Burke et al. 2020](#)).

REFERENCES

- Aerts, C., Christensen-Dalsgaard, J., & Kurtz, D. W. 2010, *Asteroseismology*, Astronomy and Astrophysics Library (Springer Netherlands), doi: [10.1007/978-1-4020-5803-5](https://doi.org/10.1007/978-1-4020-5803-5)
- Aerts, C. 2021, *Reviews of Modern Physics*, 93, 015001
- Asplund, M., Grevesse, N., Sauval, A. J., & Scott, P. 2009, *Annual Review of Astronomy and Astrophysics*, 47, 481
- Astropy Collaboration, Robitaille, T. P., Tollerud, E. J., et al. 2013, *Astropy: A Community Python Package for Astronomy*. <https://arxiv.org/abs/1307.6212>
- Balbinot, E., Helmi, A., Callingham, T., et al. 2023, *Astronomy and Astrophysics*, 678, A115
- Balbinot, E., Dodd, E., Matsuno, T., et al. 2024, *Astronomy & Astrophysics*, 687, L3
- Balmforth, N. J. 1992, *Monthly Notices of the Royal Astronomical Society*, 255, 639
- Basu, S., & Hekker, S. 2020, *Frontiers in Astronomy and Space Sciences*, 7
- Beck, P. G., Bedding, T. R., Mosser, B., et al. 2011, *Science*, 332, 205
- Bedding, T. R., Mosser, B., Huber, D., et al. 2011, *Nature*, 471, 608
- Binks, A. S., & Günther, H. M. 2024, *Monthly Notices of the Royal Astronomical Society*, 533, 2162
- Bonanno, A., Corsaro, E., & Karoff, C. 2014, *Astronomy and Astrophysics*, 571, A35
- Bonanno, A., Corsaro, E., Del Sordo, F., et al. 2019, *Astronomy and Astrophysics*, 628, A106
- Brasseur, C. E., Phillip, C., Fleming, S. W., Mullally, S. E., & White, R. L. 2019, *Astrophysics Source Code Library*, ascl:1905.007

- Brown, T. M., Gilliland, R. L., Noyes, R. W., & Ramsey, L. W. 1991, *The Astrophysical Journal*, 368, 599
- Burke, C. J., Levine, A., Fausnaugh, M., et al. 2020, TESS-Point: High Precision TESS Pointing Tool, Astrophysics Source Code Library. <http://ascl.net/2003.001>
- Ceillier, T., Tayar, J., Mathur, S., et al. 2017, *Astronomy & Astrophysics*, 605, A111
- Chaplin, W. J., Lund, M. N., Handberg, R., et al. 2015, *Publications of the Astronomical Society of the Pacific*, 127, 1038
- Chaplin, W. J., Serenelli, A. M., Miglio, A., et al. 2020, *Nature Astronomy*, 4, 382
- Chiappini, C., Anders, F., Rodrigues, T. S., et al. 2015, *Astronomy & Astrophysics*, 576, L12
- Chontos, A., Huber, D., Sayeed, M., & Yamsiri, P. 2021, arXiv:2108.00582 [astro-ph]
- Claytor, Z. R., van Saders, J. L., Santos, Â. R. G., et al. 2020, *The Astrophysical Journal*, 888, 43
- Claytor, Z. R., van Saders, J. L., Cao, L., et al. 2024, *The Astrophysical Journal*, 962, 47
- Colman, I. L., Angus, R., David, T., et al. 2024, *The Astronomical Journal*, 167, 189
- Corsaro, E., Fröhlich, H. E., Bonanno, A., et al. 2013, *Monthly Notices of the Royal Astronomical Society*, 430, 2313
- Corsaro, E., Bonanno, A., Kayhan, C., et al. 2024, *Astronomy and Astrophysics*, 683, A161
- Das, P., Hawkins, K., & Jofré, P. 2020, *Monthly Notices of the Royal Astronomical Society*, 493, 5195
- Deal, M., Escobar, M. E., Vauclair, S., et al. 2017, *Astronomy & Astrophysics*, 601, A127
- Deheuvels, S., Ballot, J., Gehan, C., & Mosser, B. 2022, *A&A*, 659, A106
- Dodd, E., Callingham, T. M., Helmi, A., et al. 2023, *Astronomy and Astrophysics*, 670, L2
- Eddington, A. S. 1926, *The Internal Constitution of the Stars* (The University Press)
- El-Badry, K., Rix, H.-W., Cendes, Y., et al. 2023a, *Monthly Notices of the Royal Astronomical Society*, 521, 4323
- El-Badry, K., Rix, H.-W., Quataert, E., et al. 2023b, *Monthly Notices of the Royal Astronomical Society*, 518, 1057
- Gaia Collaboration, Brown, A. G. A., Vallenari, A., et al. 2018, *Astronomy and Astrophysics*, 616, A1
- Gaia Collaboration, Panuzzo, P., Mazeh, T., et al. 2024, *Astronomy and Astrophysics*, 686, L2
- Gaulme, P., Jackiewicz, J., Appourchaux, T., & Mosser, B. 2014, *The Astrophysical Journal*, 785, 5
- Gaulme, P., Jackiewicz, J., Spada, F., et al. 2020, *Astronomy and Astrophysics*, 639, A63
- Gilgis, A., & Mazeh, T. 2024, *Monthly Notices of the Royal Astronomical Society*, 535, L44
- Goldreich, P., & Keeley, D. A. 1977, *The Astrophysical Journal*, 211, 934
- Green, M. J., Ziv, Y., Rix, H.-W., et al. 2024, An Upper Limit on the Frequency of Short-Period Black Hole Companions to Sun-like Stars, doi: [10.48550/arXiv.2412.02082](https://doi.org/10.48550/arXiv.2412.02082)
- Grisoni, V., Chiappini, C., Miglio, A., et al. 2024, *Astronomy & Astrophysics*, 683, A111
- Guzik, J. A., Houdek, G., Chaplin, W. J., et al. 2016, *The Astrophysical Journal*, 831, 17
- Hart, K., Shappee, B. J., Hey, D., et al. 2023, ASAS-SN Sky Patrol V2.0, doi: [10.48550/arXiv.2304.03791](https://doi.org/10.48550/arXiv.2304.03791)
- Hekker, S. 2018, in *Astrophysics and Space Science Proceedings*, Vol. 49, *Asteroseismology and Exoplanets: Listening to the Stars and Searching for New Worlds*, ed. T. L. Campante, N. C. Santos, & M. J. P. F. G. Monteiro, 95
- Henneco, J., Schneider, F. R. N., Hekker, S., & Aerts, C. 2024, *Astronomy & Astrophysics*, 690, A65
- Hon, M., Huber, D., Kuszewicz, J. S., et al. 2021, *The Astrophysical Journal*, 919, 131
- Hon, M., Li, Y., & Ong, J. 2024, *The Astrophysical Journal*, 973, 154
- Huber, D., Bedding, T. R., Stello, D., et al. 2011, *The Astrophysical Journal*, 743, 143
- Huber, D., White, T. R., Metcalfe, T. S., et al. 2022, *The Astronomical Journal*, 163, 79
- Huber, D., Slumstrup, D., Hon, M., et al. 2024, *The Astrophysical Journal*, 975, 19
- Huber, D. 2018, in *Asteroseismology and Exoplanets: Listening to the Stars and Searching for New Worlds*, ed. T. L. Campante, N. C. Santos, & M. J. P. F. G. Monteiro, *Astrophysics and Space Science Proceedings* (Cham: Springer International Publishing), 119–135
- Hurley, J. R., Tout, C. A., & Pols, O. R. 2002, *MNRAS*, 329, 897
- Hut, P. 1981, *A&A*, 99, 126
- Jermyn, A. S., Bauer, E. B., Schwab, J., et al. 2023, *ApJS*, 265, 15
- Kervella, P., Panuzzo, P., Gallenne, A., et al. 2025, *Astronomy & Astrophysics*, 695, L1
- Kjeldsen, H., & Bedding, T. R. 1995, *Astronomy and Astrophysics*, 293, 87
- Kochanek, C. S., Shappee, B. J., Stanek, K. Z., et al. 2017, *Publications of the Astronomical Society of the Pacific*, 129, 104502
- Kotko, I., Banerjee, S., & Belczynski, K. 2024, *Monthly Notices of the Royal Astronomical Society*, 535, 3577
- Kurtz, D. 2022, *Asteroseismology across the HR Diagram*, arXiv, doi: [10.48550/arXiv.2201.11629](https://doi.org/10.48550/arXiv.2201.11629)
- Lai, D. 2012, *MNRAS*, 423, 486
- Li, T., Li, Y., Bi, S., et al. 2022a, *ApJ*, 927, 167
- Li, Y., Bedding, T. R., Murphy, S. J., et al. 2022b, *Nature Astronomy*, 6, 673

- Li, Z., Zhu, C., Lu, X., et al. 2024, *The Astrophysical Journal*, 975, L8
- Li, Y., Huber, D., Ong, J. M. J., et al. 2025, K-Dwarf Radius Inflation and a 10-Gyr Spin-down Clock Unveiled through Asteroseismology of HD~219134 from the Keck Planet Finder, doi: [10.48550/arXiv.2502.00971](https://doi.org/10.48550/arXiv.2502.00971)
- Lin, W.-X., Qian, S.-B., Zhu, L.-Y., Liao, W.-P., & Li, F.-X. 2024, *The Astronomical Journal*, 168, 27
- Lu, Y., Colman, I. L., Sayeed, M., et al. 2024, Evidence of Truly Young High- α Dwarf Stars, doi: [10.48550/arXiv.2410.02962](https://doi.org/10.48550/arXiv.2410.02962)
- Lundkvist, M. S., Huber, D., Silva Aguirre, V., & Chaplin, W. J. 2018, Using Asteroseismology to Characterise Exoplanet Host Stars, doi: [10.48550/arXiv.1804.02214](https://doi.org/10.48550/arXiv.1804.02214)
- Mackereth, J. T., Miglio, A., Elsworth, Y., et al. 2021, *Monthly Notices of the Royal Astronomical Society*, 502, 1947
- Marín Pina, D., Rastello, S., Gieles, M., et al. 2024, *Astronomy and Astrophysics*, 688, L2
- Martig, M., Rix, H.-W., Silva Aguirre, V., et al. 2015, *Monthly Notices of the Royal Astronomical Society*, 451, 2230
- Miglio, A., Chiappini, C., Mackereth, J. T., et al. 2021, *Astronomy and Astrophysics*, 645, A85
- Miller, A. M., Stephan, A. P., & Martin, D. V. 2024, *Monthly Notices of the Royal Astronomical Society*, 534, 1339
- Morháč, M. 2006, *Nuclear Instruments and Methods in Physics Research Section A: Accelerators, Spectrometers, Detectors and Associated Equipment*, 559, 119
- Nielsen, M. B., Ball, W. H., Standing, M. R., et al. 2020, *Astronomy & Astrophysics*, 641, A25
- Nielsen, M. B., Davies, G. R., Ball, W. H., et al. 2021, *AJ*, 161, 62
- Ong, J. M. J., & Basu, S. 2019, *The Astrophysical Journal*, 885, 26
- Ong, J. M. J., Hon, M. T. Y., Soares-Furtado, M., et al. 2024, *The Astrophysical Journal*, 966, 42
- Ong, J. M. J., Lindsay, C. J., Reyes, C., Stello, D., & Roxburgh, I. W. 2025, *The Astrophysical Journal*, 980, 199
- Paxton, B., Bildsten, L., Dotter, A., et al. 2011, *ApJS*, 192, 3
- Paxton, B., Cantiello, M., Arras, P., et al. 2013, *ApJS*, 208, 4
- Paxton, B., Marchant, P., Schwab, J., et al. 2015, *ApJS*, 220, 15
- Paxton, B., Schwab, J., Bauer, E. B., et al. 2018, *ApJS*, 234, 34
- Paxton, B., Smolec, R., Schwab, J., et al. 2019, *ApJS*, 243, 10
- Phillips, A., Kochanek, C. S., Jayasinghe, T., et al. 2024, *MNRAS*, 527, 5588
- Pinsonneault, M. H., Elsworth, Y., Epstein, C., et al. 2014, *The Astrophysical Journal Supplement Series*, 215, 19
- Pinsonneault, M. H., Elsworth, Y. P., Tayar, J., et al. 2018, *The Astrophysical Journal Supplement Series*, 239, 32
- Pinsonneault, M. H., Zinn, J. C., Tayar, J., et al. 2024, APOKASC-3: The Third Joint Spectroscopic and Asteroseismic Catalog for Evolved Stars in the Kepler Fields, doi: [10.48550/arXiv.2410.00102](https://doi.org/10.48550/arXiv.2410.00102)
- Planck Collaboration, Ade, P. A. R., Aghanim, N., et al. 2016, *A&A*, 594, A13
- Pojmanski, G. 1997, *Acta Astronomica*, 47, 467
- Raithel, C. A., Sukhbold, T., & Özel, F. 2018, *The Astrophysical Journal*, 856, 35
- Reimers, D. 1975, *Memoires of the Societe Royale des Sciences de Liege*, 8, 369
- Ricker, G. R., Winn, J. N., Vanderspek, R., et al. 2014, *Journal of Astronomical Telescopes, Instruments, and Systems*, 1, 014003
- . 2015, *Journal of Astronomical Telescopes, Instruments, and Systems*, 1, 014003
- Rui, N. Z., & Fuller, J. 2021, *Monthly Notices of the Royal Astronomical Society*, 508, 1618
- Rui, N. Z., & Fuller, J. 2024, *The Open Journal of Astrophysics*, 7, 81
- Salaris, M., Chieffi, A., & Straniero, O. 1993, *The Astrophysical Journal*, 414, 580
- Sayeed, M., Ness, M. K., Montet, B. T., et al. 2024, *The Astrophysical Journal*, 964, 42
- Schofield, M., Chaplin, W. J., Huber, D., et al. 2019, *The Astrophysical Journal Supplement Series*, 241, 12
- Sharma, S., Stello, D., Bland-Hawthorn, J., Huber, D., & Bedding, T. R. 2016, *The Astrophysical Journal*, 822, 15
- Shibahashi, H. 1979, *PASJ*, 31, 87
- Silva Aguirre, V., Bojsen-Hansen, M., Slumstrup, D., et al. 2018, *Monthly Notices of the Royal Astronomical Society*, 475, 5487
- Smith, K. W., Smartt, S. J., Young, D. R., et al. 2020, *Publications of the Astronomical Society of the Pacific*, 132, 085002
- Stello, D., & Sharma, S. 2022, *Research Notes of the AAS*, 6, 168
- Sukhbold, T., Ertl, T., Woosley, S. E., Brown, J. M., & Janka, H.-T. 2016, *The Astrophysical Journal*, 821, 38
- Tanikawa, A., Cary, S., Shikauchi, M., Wang, L., & Fujii, M. S. 2024, *Monthly Notices of the Royal Astronomical Society*, 527, 4031
- Tassoul, M. 1980, *The Astrophysical Journal Supplement Series*, 43, 469
- Tayar, J., Claytor, Z. R., Huber, D., & van Saders, J. 2022, *The Astrophysical Journal*, 927, 31
- Tayar, J., Carlberg, J. K., Aguilera-Gómez, C., & Sayeed, M. 2023, *The Astronomical Journal*, 166, 60
- Tonry, J. L., Denneau, L., Heinze, A. N., et al. 2018, *PASP*, 130, 064505
- Tonry, J. L., Denneau, L., Heinze, A. N., et al. 2018, *Publications of the Astronomical Society of the Pacific*, 130, 064505
- Townsend, R., Teitler, S., & Paxton, B. 2013, *Proceedings of the International Astronomical Union*, 9, 505
- Ulrich, R. K. 1986, *The Astrophysical Journal*, 306, L37
- Unno, W., Osaki, Y., Ando, H., Saio, H., & Shibahashi, H. 1989, Nonradial oscillations of stars
- van Saders, J. L., & Pinsonneault, M. H. 2013, *ApJ*, 776, 67

- Vinícius, Z., Barentsen, G., Hedges, C., Gully-Santiago, M., & Cody, A. M. 2018, KeplerGO/Lightkurve
- Vrard, M., Mosser, B., & Samadi, R. 2016, *A&A*, 588, A87
- White, T. R., Bedding, T. R., Stello, D., et al. 2011, *The Astrophysical Journal*, 743, 161
- Ying, J. M., Chaboyer, B., Boudreaux, E. M., et al. 2023, *The Astronomical Journal*, 166, 18
- Yu, J., Huber, D., Bedding, T. R., et al. 2018, *The Astrophysical Journal Supplement Series*, 236, 42
- Yu, J., Casagrande, L., Ciucă, I., et al. 2024, *Monthly Notices of the Royal Astronomical Society*, 530, 2953
- Zahn, J. P. 1977, *A&A*, 57, 383
- Zhang, M., Xiang, M.-S., Zhang, H.-W., et al. 2021, *The Astrophysical Journal*, 922, 145
- Zinn, J. C., Stello, D., Elsworth, Y., et al. 2022, *The Astrophysical Journal*, 926, 191